energies

MDPI

Article

Robust LFC Strategy for Wind Integrated Time-Delay Power System Using EID Compensation

Fang Liu *, **Kailiang Zhang** and **Runmin Zou**

School of Automation, Central South University, Changsha 410083, China
* Correspondence: csuliufang@csu.edu.cn; Tel.: +86-731-88876750

Received: 5 June 2019; Accepted: 7 August 2019; Published: 21 August 2019

Abstract: This paper presents an active disturbance rejection control (ADRC) technique for load frequency control of a wind integrated power system when communication delays are considered. To improve the stability of frequency control, equivalent input disturbances (EID) compensation is used to eliminate the influence of the load variation. In wind integrated power systems, two area controllers are designed to guarantee the stability of the overall closed-loop system. First, a simplified frequency response model of the wind integrated time-delay power system was established. Then the state-space model of the closed-loop system was built by employing state observers. The system stability conditions and controller parameters can be solved by some linear matrix inequalities (LMIs) forms. Finally, the case studies were tested using MATLAB/SIMULINK software and the simulation results show its robustness and effectiveness to maintain power-system stability.

Keywords: load frequency control (LFC); equivalent input disturbance (EID); active disturbance rejection control (ADRC); wind; linear matrix inequalities (LMI)

---

1. Introduction

Load frequency control (LFC) plays a key role when it comes to measuring the power supply quality of a power system. Ensuring that the frequency is controlled at a fixed value or with small changes in its vicinity is a basic requirement of LFC [1]. In order to maintain the system frequency, some control techniques for power systems have been adopted in LFC such as an adaptive fuzzy logic approach [2], neutral network [3], and robust H_∞ control [4]. Different from conventional energy sources, wind energy has the intrinsic intermittence and fluctuation, which will inevitably bring serious influence on the frequency regulation of a power system [5]. Due to the intermittence of wind power, the large-scale wind power grid operation will affect the stability and balance of power systems [6]. Recently, the LFC problem with wind power sources has attracted much attention. With more and more wind power integrated in power systems, the LFC issue of power systems has become more difficult than before. Therefore, designing an advanced LFC strategy for the wind power generations is of significant value to ensure the stable operation of power systems under the stochastic disturbances of wind power and the random load variation. For multi-area power systems in the presence of wind turbines, a LFC design using the model predictive control (MPC) technique is proposed [7]. In [8], a linear active disturbance rejection control method was applied to power systems with high penetration of wind power. Under the condition of wind speed fluctuation, the linear active disturbance rejection technique has a more prominent control effect than the traditional control method in the doubly-fed wind turbines, which reduces the adjustment time and overshoot [9]. To solve the nonlinearities in the LFC issue of the interconnected power systems, the hybrid neuro-fuzzy scheme was applied in [10]. A low-frequency damping control strategy of a doubly-fed induction generator based on transient energy function analysis of oscillation was proposed in [11].

With the reform of power marketization, the scale of a power system gradually expands, and LFC needs to carry out wide-area information exchange or experience a large amount of data in non-dedicated communication network, which inevitably brings the problem of time delay [12]. A sliding mode control and a robust predictive control strategy for power systems with time-delay and uncertainties of parameter are presented in [13,14] respectively. The authors of [15,16] studied the impulsive control of a nonlinear dynamic system. Considering the time-varying delays, two impulsive control algorithms were designed for the islanded micro-grids in [17]. The delay correlation stability of a LFC scheme is studied by means of the Lyapunov-theory and linear matrix inequality (LMIs) techniques in [18]. The authors of [19] studied the LFC for power systems with communication delays via an event-triggered control method. In [20], a new criterion for the delay-related stability was proposed when the network multi-area LFC system was subjected to an unknown time variant exogenous load disturbance. Time delay not only reduces the control effect of the original LFC, but also makes the controller malfunction, causing the instability of the system and damaging the safe operation of the power grid. Therefore, designing a robust LFC strategy which can perfectly compensate for the influence of time delay becomes an increasingly valuable solution of the wind integrated power system [21].

In this paper, the influence of wind power integration on load frequency of a power system was studied, and the influence of communication delay on the whole system was also considered. An active disturbance rejection control (ADRC) based on equivalent input disturbances (EID) compensation for load frequency control was proposed for a wide integrated power system when communication delays were considered, applied to a two-area power system to dampen its low frequency oscillation. The disturbance information was obtained through the full-order state observer, and the disturbance estimator was designed to compensate for the disturbance. Thus, the disturbance rejection performance of the whole control system was improved.

The remaining sections of this paper are structured as follows: In Section 2, simplified wind turbine models for frequency studies are introduced. In Section 3, ADRC design strategies based on EID are discussed. Some case studies are introduced in Section 4, and the conclusions are drawn in Section 5.

2. System Modelling

Figure 1 shows a two-area interconnected wind integrated power system with two conventional generator units in each area, one aggregated wind turbine model and two controllers based on EID. In the following analysis, the basic parameter description will be listed. The notation Δ indicates the deviation from the normal state.

Currently, the variable speed wind turbine (VSWT) is the most popular type of modern wind turbine. There is a more detailed description of VSWT in [22]. Figure 2 shows a simplified frequency response model of a wind turbine based on doubly-fed induction generator (DFIG).

The structure of this model can be described by the following equations [22]:

$$\mathrm{i}_{qr} = -\left(\frac{1}{T_1}\right)i_{qr} + \left(\frac{X_2}{T_1}\right)V_{qr} \tag{1}$$

$$\dot{w} = -\left(\frac{X_3}{M_t}\right)i_{qr} + \left(\frac{1}{M_t}\right)T_m \tag{2}$$

$$p_e = wX_3 i_{qr} \tag{3}$$

by linearizing, Equation (3) can be rewritten as:

$$p_e = w_{opt} X_3 i_{qr} \tag{4}$$

$$T_e = i_{qs} = -\frac{L_m}{L_{ss}} i_{qr} \tag{5}$$

where w_{opt} is the operating point of the rotational speed, T_e is the electromagnetic torque, T_m is the mechanical power change, ω is the rotational speed, P_e is the active power of the wind turbine, i_{qr} is the q-axis component of the rotor current, V_{qr} is the q-axis component of the rotor voltage and M_t is the equivalent inertia constant of the wind turbine.

The main parameters in Figure 2 can be observed from Table 1.

$$L_0 = L_{rr} + \frac{L_m^2}{L_{ss}}, \quad L_{ss} = L_s + L_m,\ L_{rr} = L_{rs} + L_m$$

where L_m is the magnetizing inductance,R_r and R_s are the rotor and stator resistances, respectively.

L_r and L_s are the rotor and stator leakage inductances, respectively, L_{rr} and L_{ss} are the rotor and stator self-inductances, respectively, w_s is the synchronous speed.

Since each subsystem is connected by power flow through a tie line, a LFC system of each area of the two-area power system should not ignore the control of the interchange power and local frequency with the other control area. Therefore, we take the tie-line power signal into account in the dynamic LFC system model and describes a frequency model for any area i of N power system control areas with an aggregated generator unit in each area [11].

Table 1. Parameters for Figure 1.

X_2	X_3	T_1
$\frac{1}{R_r}$	$\frac{L_m}{L_{ss}}$	$\frac{L_0}{w_s R_s}$

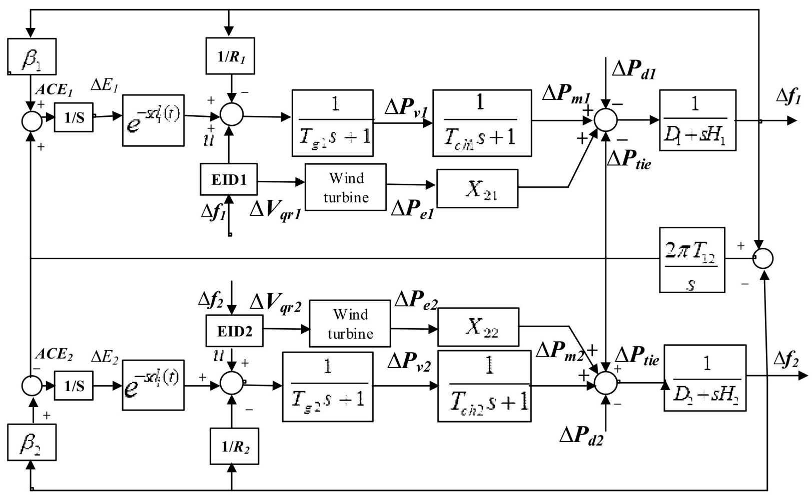

Figure 1. A two-area wind integrated power system for equivalent input disturbances (EID) based load frequency control (LFC).

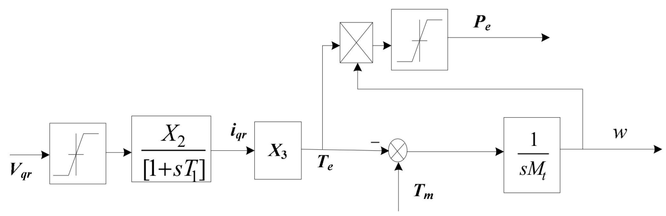

Figure 2. Simplified frequency response model of wind turbine base on doubly-fed induction generator (DFIG).

The LFC dynamic model of one area of the interconnected power system, shown in Figure 3, can be described as follows:

$$\begin{cases} \Delta\dot{f}_i = -\frac{D_i}{M_i}\Delta f_i + \frac{1}{M_i}\Delta P_{mi} - \frac{1}{M_i}\Delta P_{tie,i} + \frac{1}{M_i}\Delta P_e - \frac{1}{M_i}\Delta P_{di} \\ \Delta\dot{P}_{mi} = -\frac{1}{T_{chi}}\Delta P_{mi} + \frac{1}{T_{chi}}\Delta P_{vi} \\ \Delta\dot{P}_{vi} = -\frac{1}{R_i T_{gi}}\Delta f_i - \frac{1}{T_{gi}}\Delta P_{vi} - \frac{\Delta E(t-d)}{T_{gi}} + \frac{1}{T_{gi}}\Delta P_{ref} \\ \Delta\dot{P}_{tie,i} = 2\pi\left(\sum\limits_{j=1,j\neq i}^{N} T_{ij}\Delta f_i - \sum\limits_{j=1,j\neq i}^{N} T_{ij}\Delta f_j\right) \\ \Delta\dot{E}_i = ACE_i \end{cases} \tag{6}$$

Additionally, ΔE_i is the area control error (ACE) integral control.

$$\Delta E_i = \int_0^t ACE(s)ds \tag{7}$$

For a multi-area LFC system, the ACE is essentially composed of a regional frequency deviation and a power deviation of the line, and its calculation formula is as follows:

$$ACE_i = \Delta P_{tie,i} + \beta_i \Delta f_i \tag{8}$$

where β_i is the frequency deviation coefficient of the control area, Δf_i is the frequency deviation of area i, $\Delta P_{tie,i}$ is the tie-line power change of area i.

ΔV_i is the control area interface:

$$\Delta V_i = \sum_{i=1,j\neq i}^{N} T_{ij}\Delta f_j \tag{9}$$

where Δf is the frequency deviation, ΔP_m is the generator mechanical power deviation, ΔP_v is the turbine value position deviation, ΔP_d is the load deviation, M and D denote inertia moment and damping coefficient of generator, respectively, T_g, T_{ch} and R denote the governor's time constant, turbine's time constant and speed drop, respectively.

Furthermore, the above equations can be combined in the following state-space model:

$$\begin{cases} \dot{x}_i(t) = A_i x_i(t) + A_{di} x_i(t-d) + B_i u_i(t) + B_{wi} w_i(t) \\ y_i(t) = C_i x_i(t) \end{cases} \tag{10}$$

where

$$x_i(t) = \begin{bmatrix} \Delta f_i & \Delta P_{mi} & \Delta P_{vi} & \Delta E_i & \Delta P_{tie,i} & \Delta i_{qr} & \Delta W \end{bmatrix}^T$$

$$A_i = \begin{bmatrix} -\frac{D_i}{M_i} & \frac{1}{M_i} & 0 & 0 & \frac{-1}{M_i} & \frac{X_3 W_{opt}}{M_i} & 0 \\ 0 & \frac{-1}{T_{chi}} & \frac{1}{T_{chi}} & 0 & 0 & 0 & 0 \\ -\frac{1}{R_i T_{gi}} & 0 & \frac{-1}{T_{gi}} & 0 & 0 & 0 & 0 \\ \beta_i & 0 & 0 & 0 & 1 & 0 & 0 \\ 2\pi\sum\limits_{j=1,j\neq i}^{N} T_{ij} & 0 & 0 & 0 & 0 & 0 & 0 \\ 0 & 0 & 0 & 0 & 0 & \frac{-1}{T_1} & 0 \\ 0 & 0 & 0 & 0 & 0 & \frac{-X_3}{M_t} & 0 \end{bmatrix},$$

$$A_{di} = \begin{bmatrix} 0&0&0&0&0&0&0 \\ 0&0&0&0&0&0&0 \\ 0&0&0&\frac{-1}{T_{gi}}&0&0&0 \\ 0&0&0&0&0&0&0 \\ 0&0&0&0&0&0&0 \\ 0&0&0&0&0&0&0 \\ 0&0&0&0&0&0&0 \end{bmatrix}, B_i = \begin{bmatrix} 0 & 0 \\ 0 & 0 \\ \frac{1}{T_{gi}} & 0 \\ 0 & 0 \\ 0 & 0 \\ 0 & \frac{X_2}{T_1} \\ 0 & 0 \end{bmatrix},$$

$$B_{wi} = \begin{bmatrix} \frac{-1}{M_i} & 0 & 0 & 0 & 0 & 0 & 0 \\ 0 & 0 & 0 & 0 & 0 & 0 & \frac{1}{M_t} \\ 0 & 0 & 0 & 0 & -2\pi & 0 & 0 \end{bmatrix}^T$$

$$C_i = \begin{bmatrix} 1 & 0 & 0 & 0 & 0 & 0 & 0 \end{bmatrix}, w_i = \begin{bmatrix} \Delta P_{di} & \Delta T_m & \Delta V_i \end{bmatrix}^T$$

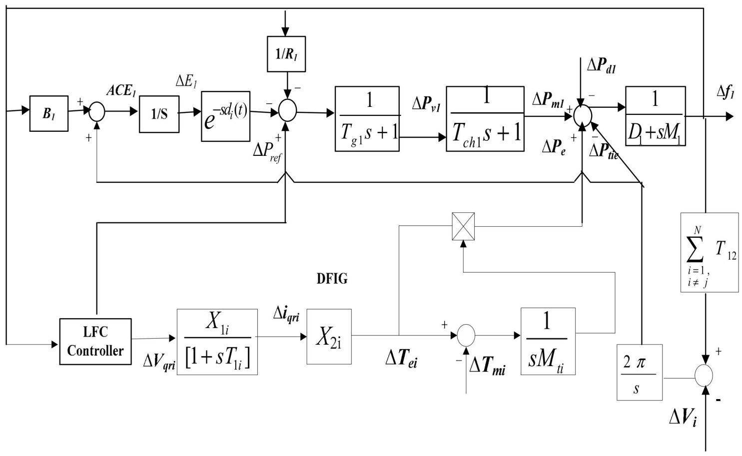

Figure 3. Dynamic model of one area of the interconnected environment.

3. ADRC Design Based on EID Compensation

This section is devoted to explaining the proposed EID-based ADRC design for the LFC. The original EID method cannot be used directly for systems with time delays, so we improved the state observer and extended the method to the time-delay system [23]. EID was originally proposed by She [24,25] and further developed by Liu [26–28]. The method is based on the idea that the effect of actual disturbance, $w(t)$, on the output of a plant (Figure 4a) can be replaced by the disturbance, $w_e(t)$, on the control input channel (Figure 4b). In Figure 4, $w(t)$ and $w_e(t)$ produced exactly the same outputs. Thus, the disturbance $w_e(t)$ is defined as EID.

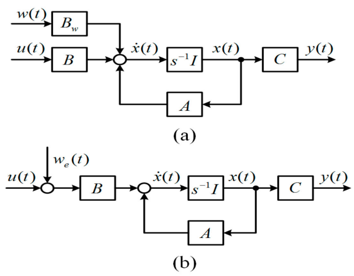

Figure 4. The concept of equivalent input disturbance, (**a**) original plant; (**b**) plant with EID.

Rewriting the plant (Equation (10)) as a plant with EID, we have

$$\begin{cases} \dot{x}\{t = Ax\{t + A_d x\{t - d + B[u[t] + w_e[t]] \\ y\{t = Cx\{t \end{cases} \tag{11}$$

Then, the system (Equation (11)) can be used to design ADRC. We constructed an EID-based closed-loop control system as in Figure 5. The system has five parts: the internal model, the state feedback controller, the disturbance estimator, the modified state observer and the control plant.

3.1. Configuration of the EID-Based Time-Delay System

In Figure 5, a new EID-based control system structure was established to achieve disturbance suppression of the wind integrated time-delay power system.

The following internal model

$$\dot{x}_R(t) = A_M x_M(t) + B_M\Big[\Delta f_{ref}[t] - y[t]\Big] \tag{12}$$

is still used to ensure accurate tracking of the reference input. When Δf_{ref} is given, A_M and B_M can be directly determined.

A full-order time-delay observer is used to estimate the EID and reconstruct the state of the controlled object, we write the state-space representation of the observer as

$$\begin{cases} \dot{\widetilde{x}}\{t = \Phi\widetilde{x}\{t + A_d\widetilde{x}\{t - d + \Psi[y[t] - C\widetilde{x}[t]] + \Gamma u_f\{t \\ \widetilde{y}\{t = T^{-1}\widetilde{x}\{t \end{cases} \tag{13}$$

where $\widetilde{x}(t)$ is the reconstruction state of $x(t)$. The gain of this full-order time-delay observer is L.

Then, we design the state-feedback controller as

$$u_f(t) = K_M x_M(t) + K_N\widetilde{x}(t) \tag{14}$$

From the above equation, we yield the disturbance estimation of the EID $\hat{w}(t)$ in Figure 5 as

$$\hat{w}(t) = B^{+}T^{-1}\Psi C[x[t] - \widetilde{x}[t]] + u_f(t) - u(t) \tag{15}$$

where $B^{+} = \left(B^T B\right)^{-1} B^T$

Since the output contains measurement noises, we used a low-pass filter to select angular frequency bandwidth for disturbance estimation. The state-space equation of the filter is described as

$$\begin{cases} \dot{x}_N\{t = A_N x_N\{t + B_N\hat{w}\{t \\ \widetilde{w}\{t = C_N x_N\{t \end{cases} \tag{16}$$

where $x_N(t)$ is the state of filter, $\widetilde{w}(t)$ is the filter disturbance estimation.

Thus, the new control law of the closed-loop control system is

$$u(t) = u_f(t) - \widetilde{w}(t) \tag{17}$$

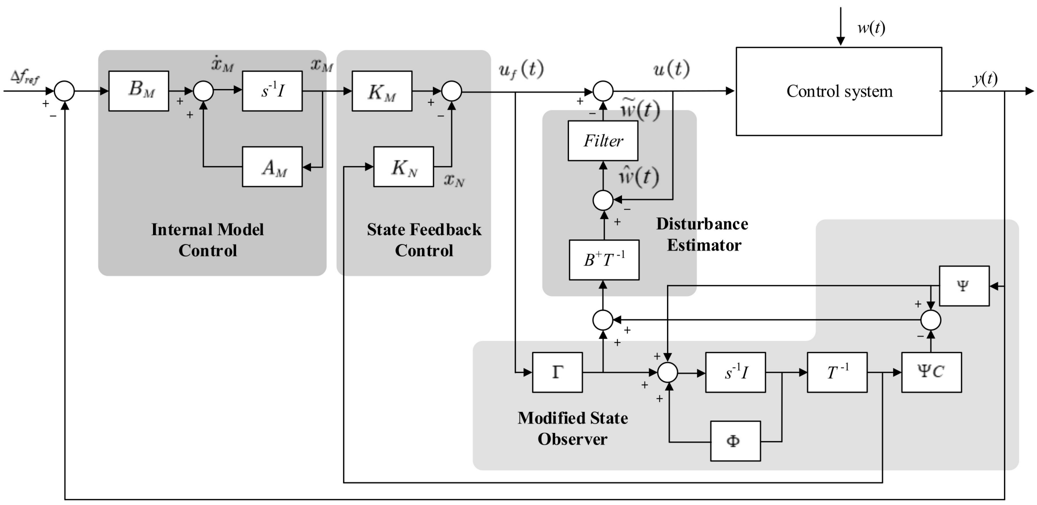

Figure 5. Configuration of the EID-based closed-loop control system.

3.2. Optimal Design of Controller Parameters

Time delay will influence the stability of the system. On account of inherent time delay, the characteristic equation of the system becomes infinitely dimensional. Thus, we propose the parameter of a controller design based on the LMI in this section.

Let $\Delta f_{ref}(t) = 0$, $w(t) = 0$. Then, the time-delay model (Equation (10)) is

$$\begin{cases} \dot{x}(t) = Ax(t) + A_d x(t-d) + Bu(t) \\ y(t) = Cx(t) \end{cases} \tag{18}$$

As shown in Figure 4, there are four states, $\widetilde{x}(t)$, $\Delta x(t)$, $x_N(t)$ and $x_M(t)$.

Define

$$\Delta x = x(t) - \widetilde{x}(t) \tag{19}$$

and describe the closed-loop system as

$$\varphi(t) = \begin{bmatrix} \widetilde{x}^T(t) & \Delta x^T(t) & {x_N}^T(t) & {x_M}^T(t) \end{bmatrix}^T \tag{20}$$

Substituting Equation (19) into (13) yields

$$\dot{\widetilde{x}}(t) = A\widetilde{x}(t) + LC\Delta x(t) + Bu_f(t) + A_d\widetilde{x}(t-d) \tag{21}$$

Combining Equations (13), (17)–(19), yields

$$\Delta\dot{x}(t) = [A - LC]\Delta x(t) - BC_N x_N(t) + A_d \Delta x(t-d) \tag{22}$$

Combining Equations (15) and (17), the filter is described as

$$\dot{x}_N(t) = B_N B^+ LC\Delta x(t) + (A_N + B_N C_N)x_N(t) \tag{23}$$

Substituting Equation (19) into (12), the internal model is obtained as:

$$\dot{x}_N(t) = B_N B^+ LC\Delta x(t) + (A_N + B_N C_N)x_N(t) \tag{24}$$

From Equations (21)–(24), the state-space representation of the control-loop system reconstructed according to EID in Figure 4, is as follows:

$$\dot{\varphi}(t) = \overline{A}\varphi(t) + \overline{B}u_f(t) + \overline{A}_d\varphi(t-d) \tag{25}$$

where

$$\overline{A} = \begin{bmatrix} A & LC & 0 & 0 \\ 0 & A - LC & -BC_N & 0 \\ 0 & B_N B^+ LC & A_N + B_N C_N & 0 \\ -B_M C & -B_M C & 0 & A_M \end{bmatrix},$$

$$\overline{A}_d = \begin{bmatrix} A_d & 0 & 0 & 0 \\ 0 & A_d & 0 & 0 \\ 0 & 0 & 0 & 0 \\ 0 & 0 & 0 & 0 \end{bmatrix}, \overline{B} = \begin{bmatrix} B^T & 0 & 0 & 0 \end{bmatrix}^T$$

The state-feedback controller law is:

$$u_f = \overline{K}\varphi(t) \tag{26}$$

where

$$\overline{K} = \begin{bmatrix} K_N & 0 & 0 & K_M \end{bmatrix}$$

Substituting Equation (26) into (25) yields the general form of time-delay system:

$$\dot{\varphi}(t) = \hat{A}\varphi(t) + \overline{A}_d\varphi(t-d) \tag{27}$$

where

$$\hat{A} = \begin{bmatrix} A+BK_N & LC & 0 & BK_M \\ 0 & A-LC & -BC_N & 0 \\ 0 & B_NB^{+}LC & A_N+B_NC_N & 0 \\ -B_MC & -B_MC & 0 & A_M \end{bmatrix}$$

3.3. Stability Analysis

Using the following Lemma 1, the time-delay power system stability analysis was carried out.

Lemma 1. *If there is a positive definite matrix Q and P, which makes the following LMI feasible, then the time-delay system (27) is asymptotically stable* [29,30].

$$\begin{bmatrix} P\hat{A}+\hat{A}^TP+Q & P\overline{A}_d \\ \overline{A}_d{}^TP & -Q \end{bmatrix} < 0 \tag{28}$$

Based on Lemma 1, the controller gain and a sufficient condition for power system stability are obtained as follows.

Theorem 1. *If there is a positive definite matrix X_1, X_{11}, X_{22}, X_3, X_4, Y_1, Y_2, Y_3 and Y_4, and suitable dimension matrices Z_1, Z_2, and Z_3, the following LMI is feasible. For a given positive parameter α and γ, the time-delay system (25) is asymptotically stable under the control law (26).*

$$\begin{bmatrix} \Phi & \Psi & X \\ \Psi^T & -Y & 0 \\ X^T & 0 & -Y \end{bmatrix} < 0 \tag{29}$$

where

$$\Phi = \begin{bmatrix} \Phi_{11} & Z_2C & 0 & \Phi_{14} \\ C^TZ_2{}^T & \Phi_{22} & \Phi_{23} & -X_2C^TB_M{}^T \\ 0 & \Phi_{23}{}^T & \Phi_{33} & 0 \\ \Phi_{14}{}^T & -B_MCX_2{}^T & 0 & \Phi_{44} \end{bmatrix},$$

$$\Psi = \begin{bmatrix} \alpha A_dY_1 & 0 & 0 & 0 \\ 0 & A_dY_2 & 0 & 0 \\ 0 & 0 & 0 & 0 \\ 0 & 0 & 0 & 0 \end{bmatrix},$$

$$X = \begin{bmatrix} \alpha X_1 & 0 & 0 & 0 \\ 0 & X_2 & 0 & 0 \\ 0 & 0 & X_3 & 0 \\ 0 & 0 & 0 & \gamma X_4 \end{bmatrix}, Y = \begin{bmatrix} Y_1 & 0 & 0 & 0 \\ 0 & Y_2 & 0 & 0 \\ 0 & 0 & Y_3 & 0 \\ 0 & 0 & 0 & Y_4 \end{bmatrix}$$

$$\Phi_{11} = \alpha AX_1 + \alpha X_1A^T + \alpha BZ_1 + \alpha Z_1{}^TB^T,$$

$$\Phi_{14} = \gamma BZ_3 - \alpha X_1C^TB_M{}^T,$$

$$\Phi_{22} = AX_2 + X_2A^T - Z_2C - C^TZ_2{}^T,$$

$$\Phi_{23} = -BC_NX_3 + C^TZ_2{}^TB^{+T}B_N{}^T,$$

$$\Phi_{33} = (A_N + B_NC_N)X_3 + X_3(A_N + B_NC_N)^T,$$

$$\Phi_{44} = \gamma A_MX_4 + \gamma X_4A_M{}^T,$$

and the singular-value decomposition of X_2 is

$$X_2 = V diag\{X_{11}, X_{22}\} V^T$$

The gain of the state feedback controller and the observer is

$$K_N = Z_1 X_1{}^{-1}, K_M = Z_3 X_4{}^{-1}, L = Z_2 U S X_{11}{}^{-1} S^{-1} U^T \tag{30}$$

Additionally, U and V can be obtained from

$$C = U[S, 0] V^T \tag{31}$$

where Equation (31) is a singular value decomposition expression of matrix C.

A detailed proof of Theorem 1 is given in [23], so we omitted the process of proof in this paper.

4. Case Studies

In this section, the proposed ADRC design based on EID compensation is evaluated using MATLAB/SIMULINK software. The basic parameter description of the model is listed in Appendix A [31]. Furthermore, the different profiles of load variation are considered to test the performance of ADRC allocated to each area.

Firstly, the effectiveness of the proposed ADRC method is verified. We study the case that both areas are without ADRC to witness the impact of time delays on two areas of power system and the other case that both areas are equipped with ADRC to confirm the effectiveness of this method. Two-area time-delay power systems with wind farm are considered. It is worth noting that the communication delay is set to be 0.2 s [32,33]. When the hysteresis power system is subjected to random load disturbance as shown in Figure 6a, from Figure 6b we can see that the frequency deviation is large and oscillating, the frequency fluctuation is beyond [−1 1] Hz after 2.2 s since the fundamental frequency of a power network is 50 Hz, and even diverges. However, the frequency fluctuations can be damped in the range of $[-0.5\ 0.5] \times 10^{-3}$ pu as shown in Figure 6c by ADRC based on EID compensation.

Next, we verify the superiority of the proposed method. The dynamic responses of wind farm time-delay power system equipped with PID controller and the proposed EID-based ADRC are shown in Figures 7 and 8. Figure 7 shows the dynamic response of frequency in Area 1 and Figure 8 shows the dynamic response of frequency in Area 2. By PID controller, the frequency is varied between $[-1\ 1] \times 10^{-3}$ pu. However, compared with PID controller, the ADRC method based on EID compensation proposed in this paper has higher stability and faster speed. As shown in Figure 7c, Δf is controlled within $[-2\ 2.5] \times 10^{-6}$ pu. Therefore, EID-based ADRC method has better robustness than the PID method.

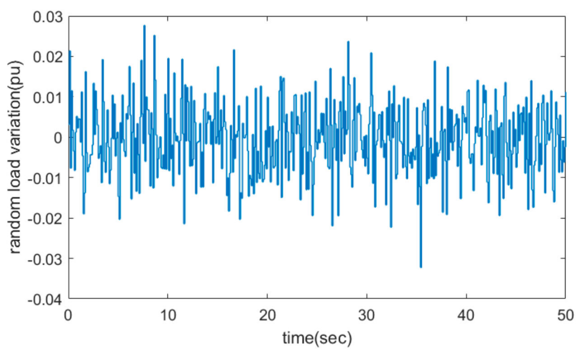

(a)

Figure 6. *Cont.*

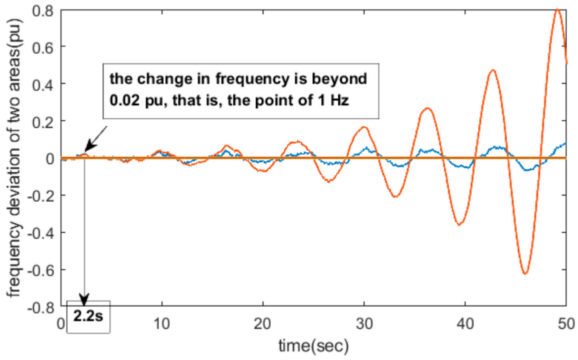

(**b**)

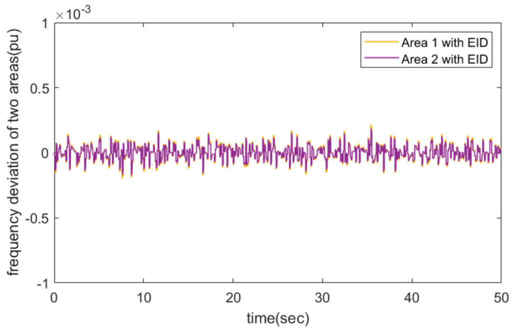

(**c**)

Figure 6. Dynamic response of two areas, (**a**) random load variation; (**b**) frequency response of two areas without ADRC; (**c**) frequency response of two areas with ADRC.

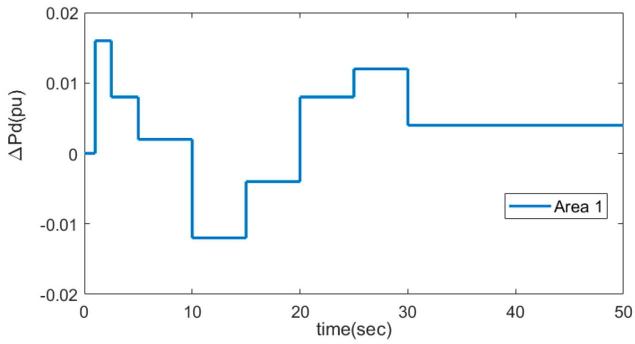

(**a**)

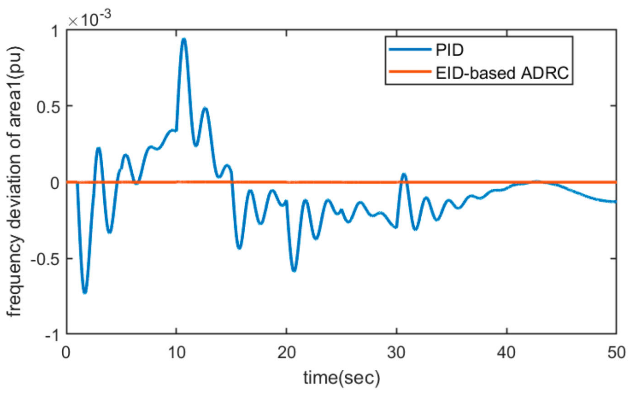

(**b**)

Figure 7. *Cont.*

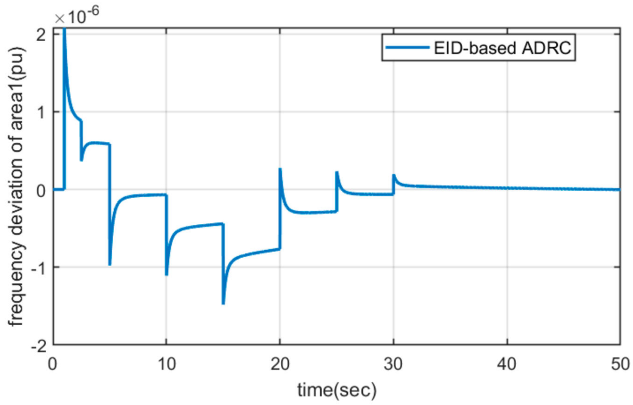

(**c**)

Figure 7. Dynamic response of Area 1, (**a**) load variation; (**b**) frequency deviations of Area 1 with different controller; (**c**) enlarged view under EID.

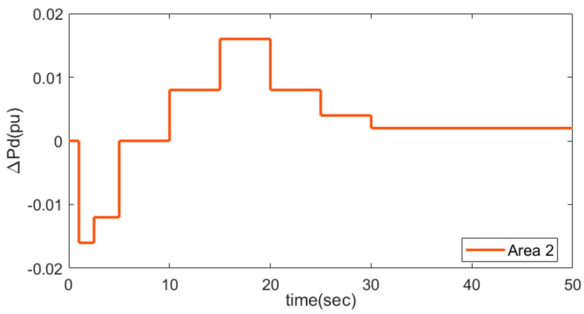

(**a**)

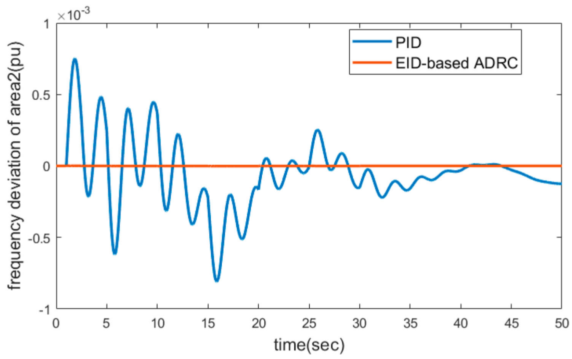

(**b**)

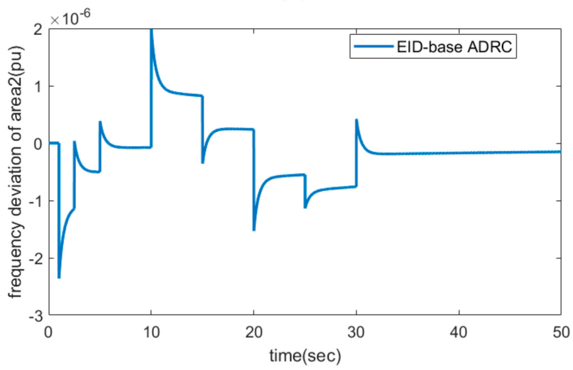

(**c**)

Figure 8. Dynamic response of Area 2, (**a**) load variation of Area 2; (**b**) frequency deviations of Area 2 with different controller; (**c**) enlarged view under EID.

When the system is disturbed by different random load as shown in Figure 9a, the dynamic performances are shown in Figure 9b–d. It can be found that the proposed strategy based on EID can enhance the frequency stability of each area and the control performance is better the PID control strategy.

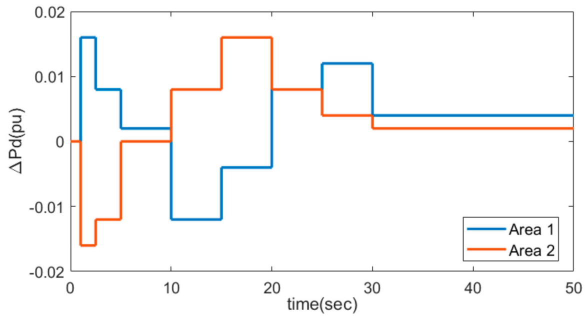

(**a**)

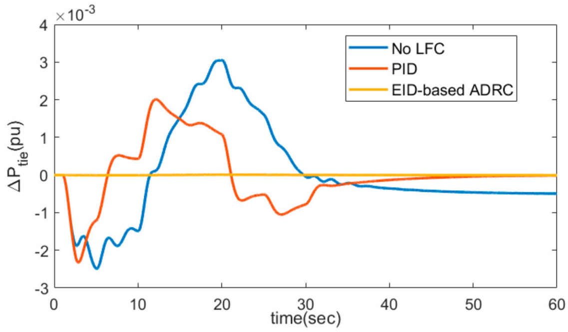

(**b**)

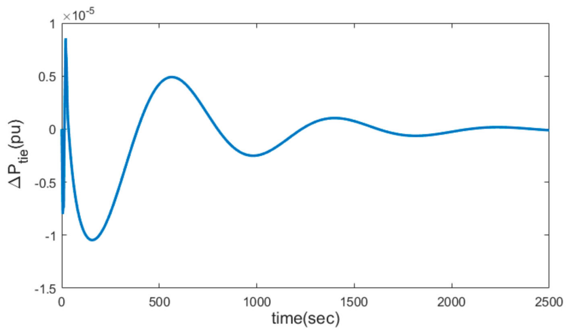

(**c**)

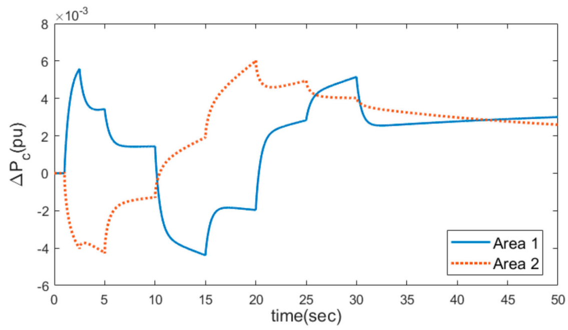

(**d**)

Figure 9. Tie-line power response of a time-delay power system with wind farm under random load, (**a**) load variation; (**b**) tie-line power deviation; (**c**) enlarged view under EID; (**d**) system control signals of EID-LFC under random load disturbance.

Figure 10 shows the simulation results with wind farm participation or without wind farm participation. It has been shown that the control system with the wind farm participation is more stable compared to the system without wind farm participation under the proposed control method.

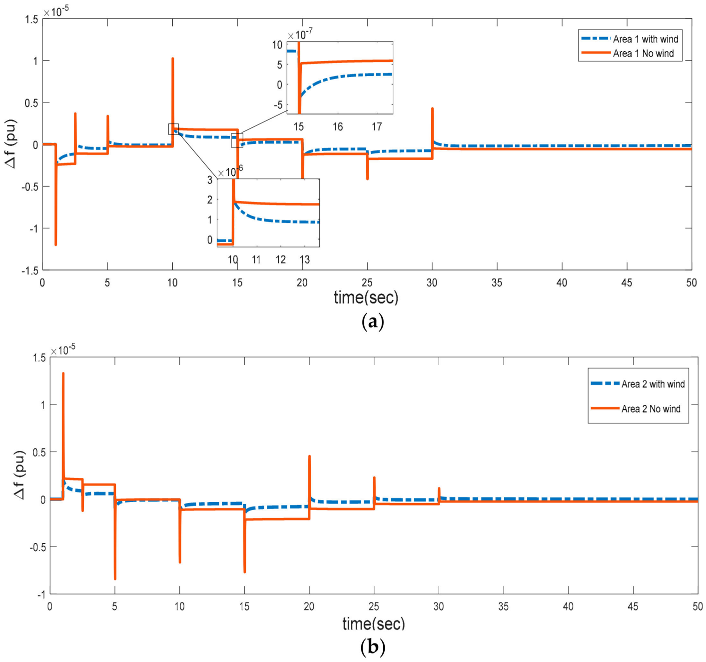

Figure 10. Dynamic response of EID with wind farm participation and EID without wind farm participation (**a**) response of Area 1; (**b**) response of Area 2.

5. Conclusions

In this article, directed at the influence of large-scale wind power integration on the security and stability of power system, and considering the impact of communication delay on this system, an ADRC method with EID compensation was applied to maintain the frequency stability of a time-delay power system with a wind farm. The LFC system model was established, and simulation results validated the effectiveness and superiority of the proposed control method. The disturbance in real time can be estimated and compensated with the control strategy based on EID. Finally, by comparing with traditional LFC methods, the simulation results show that the proposed ADRC method has a significantly higher performance at solving frequency instability under various types of load variations. The EID-based ADRC strategy can quickly and effectively suppress the influence of external disturbances on the frequency of power system.

Author Contributions: All the authors made contributions to the concept and design of the article; F.L. is the main author of this work. R.Z. provided good advice and technical guidance for the manuscript; F.L., K.Z. and R.Z. reviewed and polished the manuscript.

Funding: This work was supported by the Natural Science Foundation of China (NSFC) under Grant 61673398, in part by Natural Science Foundation of Hunan Province of China under Grant 2018JJ2529, and in part by the Huxiang Youth Talent Program of Hunan Province under Grant 2017RS3006.

Conflicts of Interest: The authors declare no conflict of interest.

Appendix A

The following is the parameters of two control area model. In addition, the coupling coefficient between these two areas is 0.1986 pu/rad.

Table A1. Parameters of two control areas.

Parameter	T_{ch} **(s)**	T_g **(s)**	R	D	β	M **(s)**
Area 1	0.3	0.1	0.05	1.0	21.0	10
Area 2	0.4	0.17	0.05	1.5	21.5	12

Table A2. Wind Turbine Parameters And Operating Point.

R_r **(pu)**	R_s **(pu)**	X_{lr} **(pu)**	X_{ls} **(pu)**	X_m **(pu)**	M_t **(pu)**
0.3	0.1	0.05	1.0	21.0	10

References

1. Sasaki, T.; Enomoto, K. Dynamic Analysis of Generation Control Performance Standards. *IEEE Power Eng. Rev.* **2002**, *22*, 54. [CrossRef]
2. Yousef, H. Adaptive fuzzy logic load frequency control of multi-area power system. *Int. J. Electr. Power Energy Syst.* **2015**, *68*, 384–395. [CrossRef]
3. Nag, S.; Philip, N. Application of Neural Networks to Automatic Load Frequency Control. In Proceedings of the International Conference on Swarm, Evolutionary, and Memetic Computing, Calcutta, India, 31 January–2 February 2014; Springer: Cham, Switzerland; Berlin/Heidelberg, Germany, 2013.
4. Chuang, N. Robust H ∞ load-frequency control in interconnected power systems. *IET Control. Theory Appl.* **2016**, *10*, 67–75. [CrossRef]
5. Kumar, A. Impact Study of Dfig Based Wind Power Penetration on Lfc of a Multiarea Power System. In Proceedings of the IEEE India Conference, New Delhi, India, 17–20 December 2015.
6. Rather, Z.H.; Chen, Z.; Thøgersen, P.; Lund, P. Dynamic Reactive Power Compensation of Large-Scale Wind Integrated Power System. *IEEE Trans. Power Syst.* **2015**, *30*, 2516–2526. [CrossRef]
7. Kunya, A.B.; Argin, M. Model Predictive Load Frequency Control of Multi-Area Interconnected Power System. In Proceedings of the 2018 IEEE Texas Power and Energy Conference, College Station, TX, USA, 8–9 February 2018; pp. 1–6.
8. Wang, S.B.; Jiang, Q.Y.; Liu, Z.Y.; Gao, Y.J. Wide-area Damping Control Considering Multiple Delays of Feedback Signals. *Autom. Electr. Power Syst.* **2008**, *32*, 18–22.
9. Yu, X.; Tomsovic, K. Application of Linear Matrix Inequalities for Load Frequency Control with Communication Delays. *IEEE Trans. Power Syst.* **2004**, *19*, 1508–1515. [CrossRef]
10. Bevrani, H.; Hiyama, T. Robust decentralized PI based LFC design for time delay power systems. *Energy Convers. Manag.* **2008**, *49*, 193–204. [CrossRef]
11. Bevrani, H. *Robust Power System Frequency Control*; Springer Science and Business Media LLC: Berlin/Heidelberg, Germany, 2014.
12. Sönmez, S.; Ayasun, S. Stability Region in the Parameter Space of PI Controller for a Single-Area Load Frequency Control System with Time Delay. *IEEE Trans. Power Syst.* **2016**, *31*, 1–2. [CrossRef]
13. Yongjuan, L.; Yang, M.; Yang, Y.; Limin, W. The study of sliding mode load frequency control for single area time delay power system. In Proceedings of the 27th Chinese Control and Decision Conference (CCDC), Qingdao, China, 23–25 May 2015.
14. Ojaghi, P.; Rahmani, M. LMI-Based Robust Predictive Load Frequency Control for Power Systems with Communication Delays. *IEEE Trans. Power Syst.* **2017**, *32*, 4091–4100. [CrossRef]
15. Li, X.; Wu, J. Sufficient stability conditions of nonlinear differential systems under impulsive control with state-dependent delay. *IEEE Trans. Autom. Control* **2017**, *63*, 306–311. [CrossRef]
16. Yang, H.; Wang, X.; Zhong, S.; Shu, L. Synchronization of nonlinear complex dynamical systems via delayed impulsive distributed control. *Appl. Math. Comput.* **2018**, *320*, 75–85. [CrossRef]
17. Lu, X.; Chen, N.; Wang, Y.; Qu, L.; Lai, J. Distributed impulsive control for islanded micro-grids with variable communication delays. *LET Control Theory Appl.* **2016**, *10*, 1732–1739. [CrossRef]
18. Jiang, L.; Yao, W.; Wu, Q.H.; Wen, J.Y.; Cheng, S.J. Delay-Dependent Stability for Load Frequency Control with Constant and Time-Varying Delays. *IEEE Trans. Power Syst.* **2012**, *27*, 932–941. [CrossRef]

19. Wen, S.; Yu, X.; Zeng, Z.; Wang, J. Event-triggering load frequency control for multi-area power systems with communication delays. *IEEE Trans. Ind. Electron.* **2015**, *63*, 1308–1317. [CrossRef]
20. Ramakrishnan, K.; Ray, G. Stability Criteria for Nonlinearly Perturbed Load Frequency Systems with Time-Delay. *IEEE J. Emerg. Sel. Top. Circuits Syst.* **2015**, *5*, 1–10. [CrossRef]
21. Zhao, S.; Gao, Z. Modified active disturbance rejection control for time-delay systems. *ISA Trans.* **2014**, *53*, 882–888. [CrossRef]
22. Mohamed, T.H.; Morel, J.; Bevrani, H.; Hiyama, T. Model predictive based load frequency control_design concerning wind turbines. *Int. J. Electr. Power Energy Syst.* **2012**, *43*, 859–867. [CrossRef]
23. Liu, F.; Xu, Z.; Li, Y.; Sidorov, D. Active disturbance rejection control based on EID compensation for LFC with communication delays. *IFAC J. Syst. Control* **2018**, *6*, 25–32. [CrossRef]
24. She, J.H.; Fang, M.; Ohyama, Y.; Hashimoto, H.; Wu, M. Improving Disturbance-Rejection Performance Based on an Equivalent-Input-Disturbance Approach. *IEEE Trans. Ind. Electron.* **2008**, *55*, 380–389. [CrossRef]
25. She, J.H.; Xin, X.; Yamaura, T. Analysis and Design of Control System with Equivalent-Input-Disturbance Estimation. In Proceedings of the 2006 IEEE International Conference on Control Applications, Munich, Germany, 4–6 October 2006; pp. 1463–1469.
26. Liu, R.J.; Wu, M.; Liu, G.P.; She, J.; Thomas, C. Active Disturbance Rejection Control Based on an Improved Equivalent-Input-Disturbance Approach. *IEEE/ASME Trans. Mechatron.* **2013**, *18*, 1410–1413. [CrossRef]
27. Liu, R.J.; Liu, G.P.; Wu, M.; Nie, Z.Y. Disturbance rejection for time-delay systems based on the equivalent-input-disturbance approach. *J. Frankl. Inst.* **2014**, *c1*, 3364–3377. [CrossRef]
28. Liu, F.; Li, Y.; Cao, Y.; She, J.; Wu, M. A Two-Layer Active Disturbance Rejection Controller Design for Load Frequency Control of Interconnected Power System. *IEEE Trans. Power Syst.* **2016**, *31*, 3320–3321. [CrossRef]
29. Gu, K.; Kharitonov, V.L.; Chen, J. *Stability of Time-Delay Systems*; Birkhauser: Boston, MA, USA, 2003.
30. Xia, Y.; Fu, M.; Shi, P. *Analysis and Synthesis of Dynamical Systems with Time-Delays*; Springer: Berlin/Heidelberg, Germany, 2009.
31. Pourmousavi, S.A.; Nehrir, M.H. Introducing Dynamic Demand Response in the LFC Model. *IEEE Trans. Power Syst.* **2014**, *29*, 1562–1572. [CrossRef]
32. Liu, J.; Yao, Q.; Liu, Y.; Yang, H. Wind Farm Primary Frequency Control Strategy Based on Wind & Thermal Power Joint Control. *Zhongguo Dianji Gongcheng Xuebao Proc. Chin. Soc. Electr. Eng.* **2017**, *37*, 3462–3469.
33. Aho, J.; Pao, L.; Fleming, P. An Active Power Control System for Wind Turbines Capable of Primary and Secondary Frequency Control for Supporting Grid Reliability. In Proceedings of the 51st AIAA Aerospace Sciences Meeting including the New Horizons Forum and Aerospace Exposition, Grapevine, TX, USA, 7–10 January 2013.